PCCP

Concentration and size effects on the size-selective particle purification method using the critical Casimir force

Journal:	*Physical Chemistry Chemical Physics*
Manuscript ID	CP-ART-11-2020-006136.R2
Article Type:	Paper
Date Submitted by the Author:	31-Jan-2021

Complete List of Authors:	Villanueva Valencia, José; University of Guanajuato, Sciences and Engineering Division Guo, Hongyu; Center for Neutron Research, National Institute of Standards and Technology Castaneda-Priego, Ramon; University of Guanajuato, Physical Engineering Liu, Yun; University of Delaware, Department of Chemical and Biomolecular Engineering; Center for Neutron Research, National Institute of Standards and Technology

Concentration and size effects on the size-selective particle purification method using the critical Casimir force

Jose Ramon Villanueva-Valencia[†, ‖], Hongyu Guo[†,‡], Ramon Castañeda-Priego[†, ‖], Yun Liu[*,†,‡]

[†] Center for Neutron Research, National Institute of Standards and Technology, Gaithersburg, Maryland 20899, USA.

[‖] Sciences and Engineering Division, University of Guanajuato, Leon, Guanajuato, 37150, Mexico.

[‡] Department of Chemical and Biomolecular Engineering, University of Delaware, Newark, Delaware 19716, USA.

KEYWORDS: Colloids, particle aggregation, critical Casimir forces, purification

ABSTRACT: Critical Casimir force (CCF) is a solvent fluctuation introduced interaction between particles dispersed in a binary solvent. Recently, it has been demonstrated that the CCF induced attraction between particles can trigger the particle size-sensitive aggregation, and has thus been used as an efficient way to purify nanoparticles by sizes. Here, combining small angle neutron scattering and dynamic light scattering, we investigate the effects of size and concentration on this particle size separation method. Increasing the particle concentration does not significantly affect the purification method, but the solvent composition needs to be adjusted for an optimized efficiency. This purification method is further demonstrated to work also very efficiently for systems with the particle size ranges from 15 nm to about 50 nm with a very large size polydispersity. These results indicate that for both short-ranged and long-ranged attraction relative to the particle diameters, the CCF introduced particle aggregation is always size sensitive. This implies that the particle aggregation is strongly affected by its size polydispersity for many colloidal systems. We further propose a method to use the light scattering to help identify the temperature range within which this particle purification method can work efficiently instead of using neutron scattering.

INTRODUCTION

Colloidal systems are commonly encountered in many materials of our everyday life, such as pharmaceutical drugs, foods, paints, and cosmetics [1, 2, 3, 4, 5, 6, 7, 8, 9] For many applications, monodispersed particles are desirable. However, majority of synthesized colloidal particles have the size polydispersity, and thus may require a post-synthesis purification of particles based on their sizes. Due to the difference of particle-particle interactions for different systems, many purification methods only work on some specific type of particles. There have been increased interests to find a generic method that may potentially work for many different types of particles.

The effective colloidal interactions between particles that dictate the aggregation and phase behavior are influenced by the combination of the direct interactions between particles and indirect effects mediated by the solvent molecules [10, 11, 12]. In the past few decades, there have been strong interests in studying the intriguing solvent mediated interaction among colloids dispersed in a binary solvent close to its liquid-liquid phase separation critical point [13, 14, 15, 6, 16, 17]. When dispersing colloidal particles with similar surface properties in a binary solvent, the density fluctuation of the binary solvent can introduce an effective attraction between colloidal particles that is sensitive to the correlation length of the solvent fluctuation. The correlation length of the bulk solvent increases when approaching the critical point [18, 19, 20]. Thus by controlling the sample temperature, a relatively long-ranged attraction among colloids can be tuned. Despite all the debates [21, 22], this type of interaction has been commonly termed as the critical Casimir forces (CCF), whose interaction strength and range depends strongly on the temperature difference away from the critical point, solvent concentration, and surface chemistry of particles [13, 14, 23, 24]. Since the pioneering work by Fisher and de Gennes [25] on the CCF between a pair of walls, great efforts have been devoted to developing theoretical frameworks in terms of universal scaling functions through the relevant thermodynamic variables [19, 20, 18], demonstrating experimental evidence of CCF[14, 15, 26, 27] and using computer simulations [6, 16, 28] to understand how this interaction affects the particle assembly.

Because this solvent fluctuation induced interaction is related with the critical phenomenon in a binary solvent, it is thus a generic interaction between colloidal particles. Recently, taking advantage of the generality of the CCF, a particle size separation method is demonstrated by using the CCF [29]. It has been observed that the CCF induced aggregation is highly sensitive to the size of the particles. The experimental evidence showed that this process is reversible, i.e., when the solution is moving far away from criticality, particle aggregates can be dissolved and recover

a homogenous solution [13, 17, 27, 24]. This particle size sensitive aggregation was used to separate particles to remove bigger particles from a solution and improve the monodispersity of nanoparticles in solution. This has been demonstrated previously for nanoparticle radius range from about 4 nm to 15 nm at relatively low particle volume fractions (≈ 0.5 % volume fraction) [29]. As the CCF is a density fluctuation induced critical phenomenon, this particle purification method can be potentially a generic method to many different kinds of particulate systems.

However, it is well-known that colloidal aggregation and phase behavior are sensitive to the relatively range of the attraction. The interaction range of the CCF is relatively long ranged in the previous study since the ratio between the interaction range and particle diameter is about 50 % for the purification conditions used in the previous cases. Even though the CCF is a generic solvent introduced interaction, it remains unclear if this size sensitive aggregation remains to be true for much larger particles where the CCF becomes relatively short-ranged. In addition, in order to improve the efficiency of this purification method, it is desirable to work with more concentrated particle solutions. However, it is still not clear how the purification method needs to be adjusted when the particle concentration increases.

To address those questions, we have investigated the purification effect for a system with much larger size, and also evaluated the effect by increasing the particle concentrations in this paper. Small Angle Neutron Scattering (SANS) and Dynamic Light Scattering (DLS) are used to study the aggregation behavior.

MATERAILS and EXPERIMENT

We have selected two kinds of silica particles: P1: Ludox SM-30 with the mean radius ≈5nm (from Sigma-Aldrich); and P2: Ludox PW-50 (polydisperse solution of particles with the radius from ≈20nm to ≈50nm purchased from Grace Davison). Both types of particles are dispersed into a well-studied binary solvent, 2,6-lutidine/water mixture. This binary solvent has a lower critical temperature at T_c=33.4 °C with the critical lutidine mole concentration at w_c= 0.0643, which corresponds to 29% mass fraction of lutidine in the lutidine/H2O mixture. Lutidine (>99.9%) was purchased from Sigma-Aldrich and used as received. Milli-Q water (18.2 MΩ cm) was used when H_2O was needed. D2O (>99.9%) was purchased from Cambridge Isotope.

Both types of silica particles, P1 and P2, favor water instead of lutidine on their surfaces. The schematic phase diagram at dilute particle solution (≤ 0.5 % particle volume fraction) is shown in Figure 1 [29]. And, due to the preferential adsorption which is associated to the boundary conditions of particle surfaces [30], the temperature-molar concentration phase diagram in which colloidal aggregation occur, is not symmetric [31, 32]. And particle aggregation appears on the side of critical mass fraction poor in the component preferred by the particle surface. So in our case, reversible aggregates promoted by the CCF are formed usually at the lutidine concentration, w, larger than w_c. Figure 1 shows the existence of a turbid supernatant solution with some precipitated aggregates in a narrow temperature range $T_a(w)<T<T_s(w)$ and $w>w_c$, which is the blue solid region in Fig. 1 (T_s is the temperature of the solvent binodal phase separation curve of the pure solvent, and T_a is the lowest temperature at which we observed precipitated aggregates at the bottom of the vial, i.e., the precipitation line).

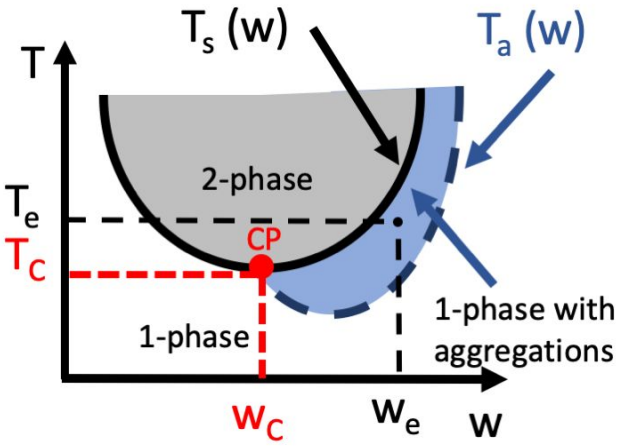

Figure 1. Schematic phase diagram of 2,6 lutidine/water mixture. The binodal is inverted in plane expanded by lutidine mole concentration (w) and Temperature (T), and has a lower critical point (CP) located at w_c=0.0643 and T_c=33.4°C, red point. See text for more details.

Two experimental systems are investigated. One is P1 silica particles at 1% volume fraction. Another one is P2 silica particles at 0.4% volume fraction. The lutidine concentration is w=0.0765 and w=0.0899 for the first and second systems, which correspond to 33% and 37% mass fraction for the lutidine/H2O mixture respectively. Other solvent compositions close to the concentrations chosen here show similar results too. The experiment was done by increasing the sample temperature to a processing temperatures, T_p, to promote the size-selective precipitation of particles for $T_p > T_a$.

Small angle neutron scattering (SANS) is used to study the size and particle aggregation. Neutrons interact with the nuclei of atoms and do not damage a sample. The contrast matching method (by mixing H_20 and D_2O) is used to match the scattering length density (SLD) of water with the SLD of lutidine so that the scattering results are dominated by the particles in solution. There is no contribution to the scattering signal by the solvent fluctuation when increasing the sample temperature. SANS experiments were performed at NGB30mSANS and nSoft 10m SANS beamlines at the NIST Center for Neutron Research (NCNR), Gaithersburg, USA. For the in-situ SANS experiment, each sample had a waiting time of 30 minutes after each temperature change to ensure that the sample temperature remains stable during a measurement. Dynamic light scattering (DLS) was conducted using DynaPro NanoStar from Wyatt Technology.

The in-situ SANS data at different temperatures can be fitted well by assuming that there are two or three independent population of polydisperse spheres in

solutions. The size distribution, *f(R)*, of radius *R* is given by the normalized Schulz distribution [33],

$$f(R) = \left[\frac{z+1}{\langle R\rangle}\right]^{z+1} R^z exp\left[-\left(\frac{z+1}{\langle R\rangle}R\right)\right]\frac{1}{\Gamma(z+1)}$$

Here, Γ is the gamma function, $\langle R\rangle$ is the mean sphere radius and z is a parameter related to the width of the distribution. In particular, one has a polydispersity index $p = \sigma_R/\langle R\rangle$, where σ_R is the root-mean-square deviation from mean size, given by $p = 1/(z+1)^{1/2}$.

Static light scattering (SLS) was used to determine T_a and find the accurate range of temperatures where aggregation particle occurs. The sample is prepared by mixing the right volume fraction of particles into the 2,6 lutidine-H_2O/D_2O solvent. The change of scattered light intensity from a sample was recorded as a function of the sample temperature. After each temperature change, there is 20 minute waiting time to allow the sample temperature to become stable before a measurement. Even though it is possible to study the in-situ aggregation with the DLS, the signal may have the contribution from the solvent fluctuation in addition to the particles in solution. The data interpretation could be potentially challenging at the temperatures close to T_s(w).

RESULTS AND DISCUSSION

As reported previously [29], the nanoparticle purification procedure using the CCF involves three steps: 1) identify the lutidine concentration of the solvent and prepare the particle solution at the temperature in the one phase region[see Fig. 1]; 2) increase the temperature slowly to the processing temperature, T_p, to be larger T_a(w), but smaller than T_s(w), to introduce the particle aggregation and let larger particles precipitate out of the solution; 3) remove the precipitates and obtain the supernatant solutions containing the particles with smaller sizes. Here, *w* is the lutidine concentration of the solvent.

The particle precipitation starts at T_a(w). But the majority of particles may precipitated out of the solution at T_e(w), which is usually much smaller than T_s(w) as shown in Fig. 1. The difference, ΔT_p(w), between T_e(w) and T_a(w), is the working temperature range for this particle purification method. Usually, we hope that the precipitation process has a wide range of temperature over T_a(w), i.e. a large ΔT_p(w), so that we can set many temperature points in this temperature region to finely control the average particle size in the supernatant. In the cases reported previously [29], ΔT_p(w) is about 1~2 °C. As many temperature control devices can have the temperature control precision at 0.1 °C or better. ΔT_p(w) with 1~2 °C range is considered a reasonable range. However, if ΔT_p(w) is too small, it becomes more difficult to have many temperature points within the particle precipitation region. Therefore, even though the proposed purification method works with a wide range of lutidine concentration, the efficiency of this purification method depends on *w* and consequently ΔT_p (w). When started working on a new system, it is important to first identify *w*, T_a(w), and ΔT_p(w). Here, we use SANS to identify the *w*, T_a(w), and ΔT_p(w) and study the efficiency of the average particle size in solutions after each purification steps.

- IN SITU SANS EXPERIMENT

In order to increase the yield of the purification method, it is desirable to work on larger particle concentrations. However, when increasing the particle concentration, the optimal lutidine concentration to have large ΔT_p(w) can be shifted. Previously, it was shown that for P1 particles at 0.4% volume fraction, ΔT_p is about 1.6 °C for *w*=0.0899,

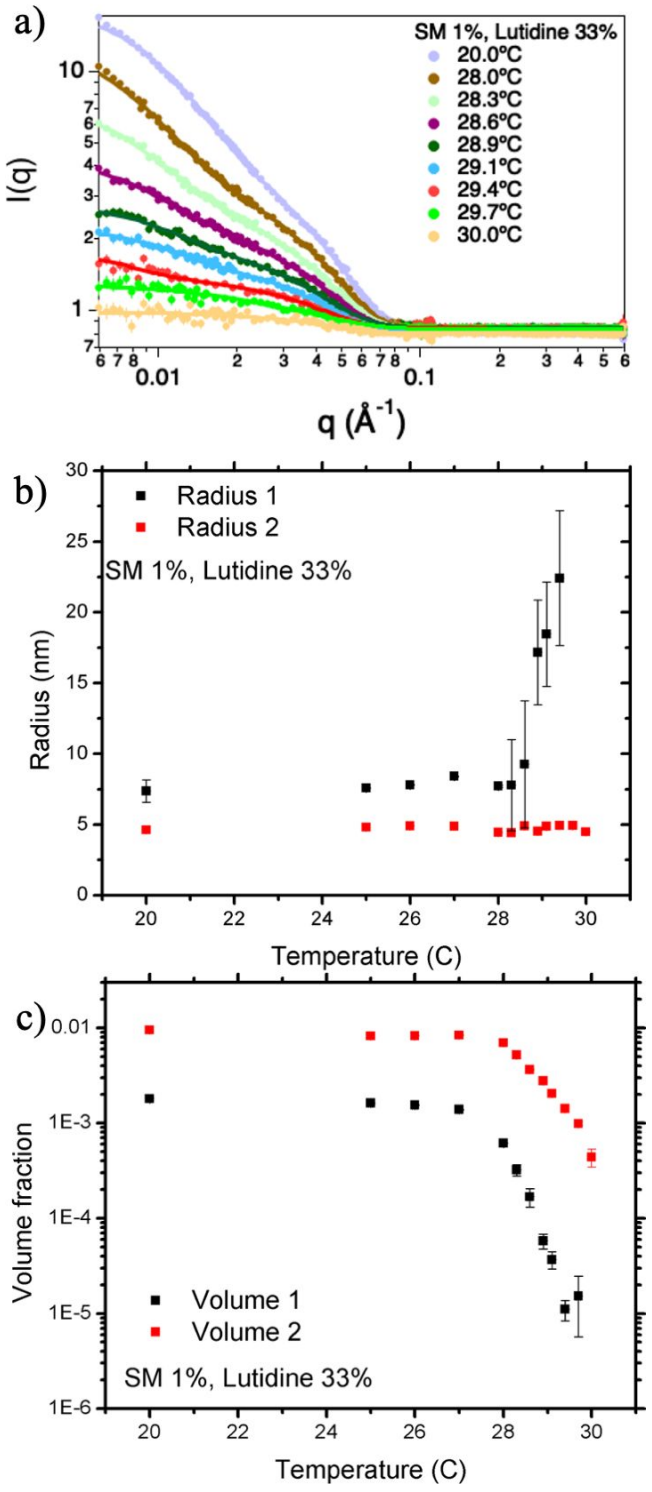

Figure 2. a) Symbols are in situ SANS scattering patterns at different temperatures for P1 particles at 1% volume fraction immersed in lutidine/water mixture at 33% mass fraction lutidine. Solid lines are the fitting results. The following results are obtained using two population Schulz distribution to obtain: b) Mean radius of P1 silica particles as a function of temperature. Radius 1 is the size for the large particle and particle aggregates. Radius 2 is the almost constant value for the small particle group. c) Volume fraction of P1 silica particles as a function of temperature. Volume 1 is the volume fraction of large particles or particle aggregates. Volume 2 is the volume fraction of small particle group. The error bars represent one standard deviation. In some cases the error bars are smaller than the symbol.

which correspond to the 37% mass fraction of lutidine in solvent [29]. In this study, we increased the particle concentration from 0.4% volume fraction to 1% volume fraction. It turns out that ΔT_p becomes smaller when increasing particle concentration. By testing different lutidine concentration in solvent, it is found smaller lutidine concentration at w=0.0765 (corresponding to 33% mass fraction of lutidine/H_2O mixture) works very well for 1% P1 volume fraction particle in solution.

To demonstrate *in situ* the structural change of our samples during the aggregation process at w=0.0765 and identify $T_a(w)$, and $\Delta T_p(w)$, SANS was used to measure the change of the average size and concentration of the particles in solution. As our goal is to focus on the structural change of dispersed colloids, we exploit the contrast variation method by mixing D_2O and H_2O, with the mole ratio M_{D2O}/M_{H2O}=0.328, to match the SLD of lutidine so that any contribution to SANS signals from the solvent density fluctuations becomes negligible when the system approach the coexistence region of the solvent.

Figure 2a) shows SANS scattering pattern for P1 silica particles at different temperatures. The scattering intensity is sensitive to the particle concentration and size distribution when changing the sample temperature. As particle precipitates are out of the neutron beam, the SANS patterns are dominated by the scattering of particles dispersed in the supernatant. At room temperature (20°C), far away from the demixing temperature of the binary solvent, the dispersed P1 particles has a broad size-distribution consistent with the previous observation. As the temperature increases step by step, the scattering intensity decreases since some particles are taken away from the supernatant due to the precipitation. The Guinier region of SANS intensity becomes flatter at higher temperature indicating that the average size of particles in the supernatant becomes smaller.

To quantitatively analyze the SANS measurements, the size distribution of particles was modeled as two populations of rigid spherical particles, respectively, consistent with the previous study [29]. One population is used to describe the group of particles which have smaller sizes and another population is used to describe the group of particles with larger sizes including also large particle aggregates that are not precipitated out of solutions. These aggregates are formed due to the CCF introduced attraction. For each population, the size distribution is described by a Schulz distribution [33], and thus has two parameters, the mean radius $\langle R\rangle$ and width $\sigma_r/\langle R\rangle$. The fitting parameters of each population are the volume fraction φ, average radius $\langle R\rangle$ and polydispersity index $p = \sigma_R/\langle R\rangle$. From the fittings of the scattering intensity in Fig. 2a) for the concentrated solution, we determine the values of volume fraction and mean radius at different temperature as shown in Figs. 2b) and 2c).

From Fig. 2b), the mean radius of large particles is about 7.5 nm while the mean radius of small particle group is about 4 nm which is consistent with the mean size of particles as observed from *in situ* SANS experiments of particles P1 in

Ref. [29]. The radius and volume fraction of each group of particles do not change notably for T < T_a. At 1% volume fraction of P1 particles with w=0.0765, T_a is about 28.3 °C. For temperatures larger than T_a, the CCF causes the formation of particle aggregates as reflected by the increase of the mean radius for large particle group shown as black squares in Fig. 2b). At the same time, there is a sharp decrease of the volume fraction of large particle group [black squares in Fig. 2c)] indicating that large particles preferentially participate in the aggregation and precipitate out of the supernatant. In the meanwhile, the radius of the small particle group [red squares in Fig. 2b)] follows almost a constant value around 4nm in all range of processing temperatures. Furthermore, its volume fraction decreases as well, but with much smaller rate, this is shown by the red squares in Fig. 2c). This indicates that the precipitates also have small particles inside. However, the relative ratio of the volume fraction between large and smaller particles in solutions decrease significantly due to the precipitation. Hence, the relative population of large particles become much smaller and the particle size distribution becomes thus narrower in the supernatant. (The error bars in Fig. 2 represent one standard deviation. In some cases the error bars are smaller than the symbols.)

Overall, increasing volume fraction of P1 particles from 0.4 % volume fraction to 1% volume fraction decreases ΔT_p at w=0.0899 since it is easier for particles to aggregate at a larger volume fraction. Thus, more particles can precipitate out of solutions at the same temperature range. However, slight decreasing the lutidine concentration to w=0.0765 can increase ΔT_p so that we can observe similar purification efficiency for 1% volume fraction similar to what was observed previously for 0.4 % volume fraction particle concentration at w=0.0899. It has been shown that the attraction strength between two particles introduced by a CCF is related with the surface layer of molecules preferentially adsorbed on a particle [17, 34, 35, 36]. The layer thickness and difference between the surface solvent concentration and the bulk concentration determine the attraction strength [37, 38]. As our particles preferentially adsorb water molecules, decreasing w can decrease the composition difference between surface and bulk solvent, and thus can decrease the strength of the attraction between particles at the same temperature range. Therefore, we can achieve larger ΔT_p by decreasing w. However, notice that decreasing w excessively may not be desirable either. When w is too small, the attraction strength may be too small. As a result, the attraction strength by the CCF may not be strong enough to generate enough aggregates to cause the precipitation. In addition, decreasing w moves T_a(w) closer to T_s(w), as can be seen in Fig. 1. Since T_a(w)< T_e(w)<T_s(w), ΔT_p may become smaller. Hence, for a given particle concentration, there is an optimum lutidine concentration, w, that could maximize ΔT_p(w).

So far, we show that the purification method works well for small nanoparticles. However, it is known that the particle size can have strong effect on the phase diagram. Particles with short-ranged attractions can have metastable liquid-liquid phase transition while systems with relatively long ranged attraction has stable liquid-liquid phase transition [39, 40]. Here, a short-ranged attraction means that the range of the attraction is only about 20% of the particle diameter or shorter [7]. Systems with short-ranged attractions have been intensively studied in the past several decades. For P1 particles, the average diameter before the purification is about 10 nm. The attraction range introduced by the CCF is

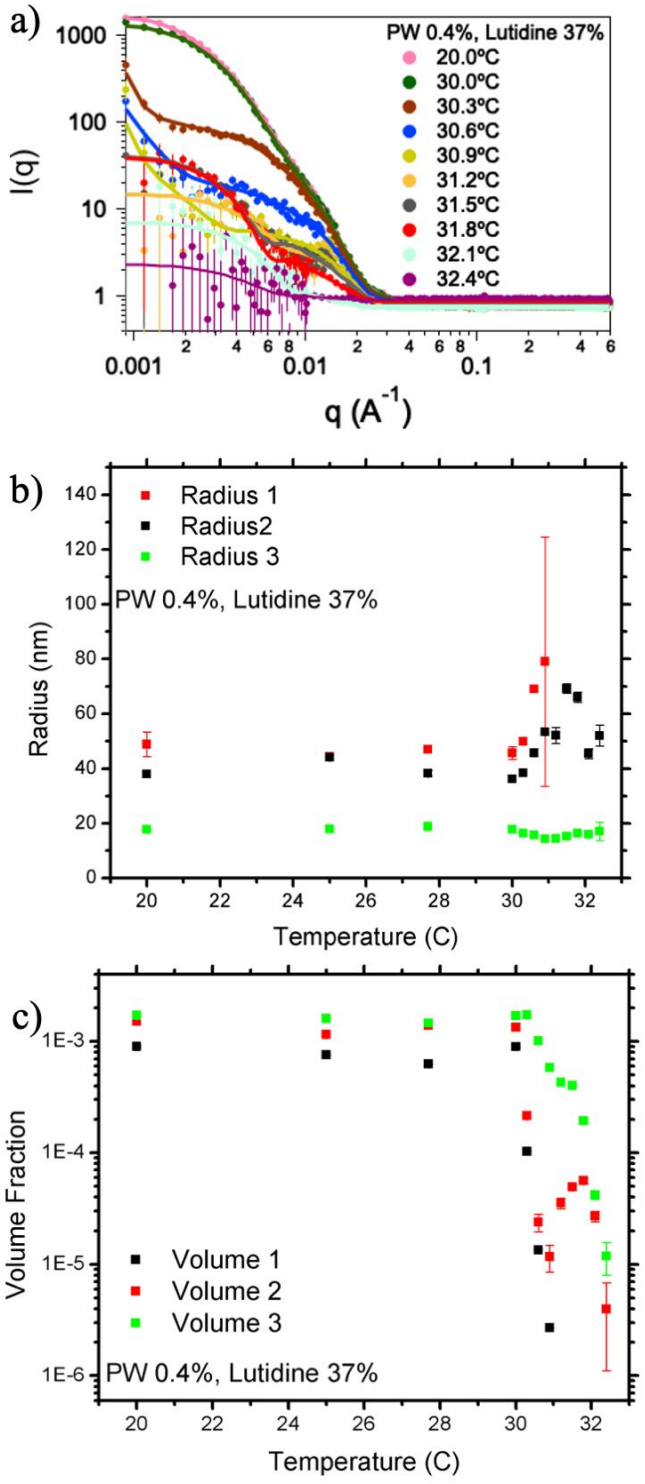

Figure 3. a) Symbols are in situ SANS scattering patterns at different temperatures for P2 particles at 0.4% volume fraction immersed in lutidine/water mixture at 37% mass fraction lutidine. Solid lines are the fitting results. The following results

are obtained using three population Schulz distribution to obtain: b) Mean radius of P2 particles as a function of temperature. Radius 1 and Radius 2 are the sizes for larger particles and particle aggregates. Radius 3 is for the smaller-sized particles the in solution. c) Volume fraction of P2 silica particles. Volume 1 and Volume 2 are the volume fraction of large particles and particle aggregates. Volume 3 is the volume fraction of the smaller-sized particles. The error bars represent one standard deviation. In some cases the error bars are smaller than the symbol.

proportional to the correlation length of the solvent. Within our temperature range, the correlation length of the solvent ranges from about 3 nm to about 6 nm. Thus for P1 particles, the average relative range of the attraction between particles in P1 system is from about 30% to about 60%. Therefore, for P1 particles, the attraction range introduced by the CCF during the purification process is not short-ranged. Hence, one interesting question is that for a system with a short-ranged attraction, will this purification method still work? To test this, we use P2 particles with the average size of about 55 nm. For the similar temperature range, the relative range of the attraction estimated based on the correlation length given above is about 11%.

Figure 3a) shows SANS scattering pattern for P2 silica particles at different temperatures. P2 particles have a wide range of the size polydispersity. Similar to that observed for P1 particles, SANS intensity decreases as the temperature increases and the intensity at low-q decrease faster than the intensity at high q indicating that more large particles are removed from the supernatant.

Therefore, for particles with very large sizes, the aggregation introduced by a short-ranged attraction is also size sensitive. The purification method based on the size sensitive aggregation still works well. This observation is very significant as it implies that this size sensitive aggregation may be a generic effect for all particle systems with a short-ranged attraction.

Due to the large size polydispersity of P2 particles in solution, three population groups: a big-sized, middle-sized and small-sized groups, are used to fit the SANS data with each group following a Schulz distribution. Figure 3b) shows that T_a is about 30.0°C for this sample. At $T < T_a$, the mixture is homogenous and the mean radius of the three populations does not change. For $T > T_a$, the CCF introduces the particle aggregation. The radius for two larger particle groups increases. At the same time, there is a sharp decrease of the volume fraction for two larger particle groups shown in Fig. 3c). Also, the radius for the smallest particle group does not change too much and its volume fraction also decrease even though the decrease rate is much smaller. The population of the final sample contains a narrow and relatively monodispersed particles with the size around R=20nm, as can be seen from green squares in Fig. 3b). The fitting results for the sample P2 show more dispersed results for particle size and volume fraction for the middle and bigger groups of particles, which is related with the larger error bars at low-q in Fig. 3a). These results clearly show that the sample P2 follows the same behavior as that of the sample P1. (The error bars in Fig. 3 represent one standard deviation, in some cases the error bars are smaller than the symbol. As very few particles are left in solution at high temperatures, the error bars for some SANS patterns are large at high temperatures as shown in Fig. 3a).)

- EX SITU EXPERIMENT

The in-situ SANS experiment helped to determine w, $T_a(w)$, and $\Delta T_p(w)$, which are key parameters for this purification method. *Ex situ* experiment is performed to purify both P1 and P2 particles by removing the larger sized particles away from the solution following the aforementioned three steps. Once the purified particles in the supernatant are obtained at different processing temperature, T_p, we performed both SANS and DLS to obtain the average size information to evaluate the size change of a sample as a function of T_p.

The *ex situ* experiment was performed in the following way. Once a given sample is prepared in the one phase region at the temperature below $T_a(w)$, we warm up the sample to different processing temperatures, T_p. The precipitates and supernatant containing purified particles are then separated. And the supernatant is then cooled to room temperature. The solvents of all samples from the supernatant were further exchanged with H_2O. (This step was necessary to get the information of solution viscosity and refractive index, which are essential to obtain the hydrodynamic radius, R_h, using DLS.) SANS is also used to measure these samples to obtain the radius of gyration, R_g, of the purified particles.

For the Guinier region of a SANS pattern, $I(Q) \approx I_0 e^{-\frac{1}{3}Q^2R_g^2}$. R_g can thus be obtained by fitting the SANS patterns. One example is shown in Fig. 4 for P1 particle purified at T_p=28.7°C with R_g=9.21±0.18 nm. R_g (red squares) for both P1 and P2 samples at different processing temperatures are shown in Figs. 5a) and 5b) respectively. Similar to the *in situ* study, at temperatures below T_a, R_g does not change significantly. As the processing temperature increase and enters to the aggregation region, larger particles prefer to form aggregates and precipitate out of the solution and R_g starts to decrease monotonically as a consequence of purification process.

DLS was also used to obtain the average hydrodynamic radius since the diffusion coefficient based on the Stokes-Einstein equation can be extracted from the decay rate by fitting the measured intensity autocorrelation function with an exponential function. The measured R_h (black squares) for both experimental systems are displayed in Figs. 5a) and 5b). The change of R_h follows the same trend as that of R_g, confirming that this purification procedure improves the monodispersity of purified samples. (The error bars in Fig. 5 represent one standard deviation. In some cases the error bars are smaller than the symbol. The large error bars at high temperatures are due to the weak scattering intensity from very small population of particles left in the solution.)

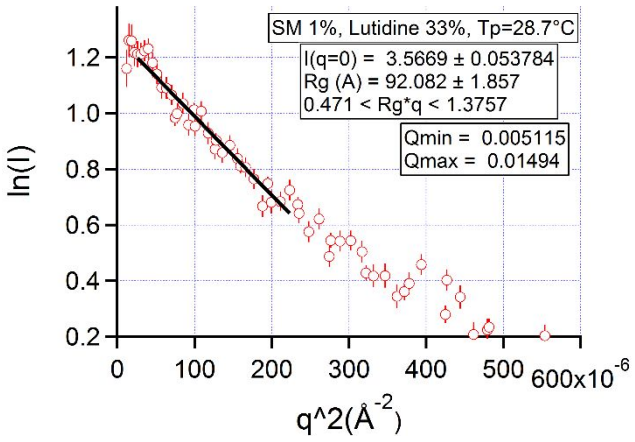

Figure 4. Guinier plot for P1 silica particles measured at room temperature after processed at T_p=28.7°C. The black solid line shows the linear fitting to give rise R_g=9.21±0.18nm. The error bars represent one standard deviation.

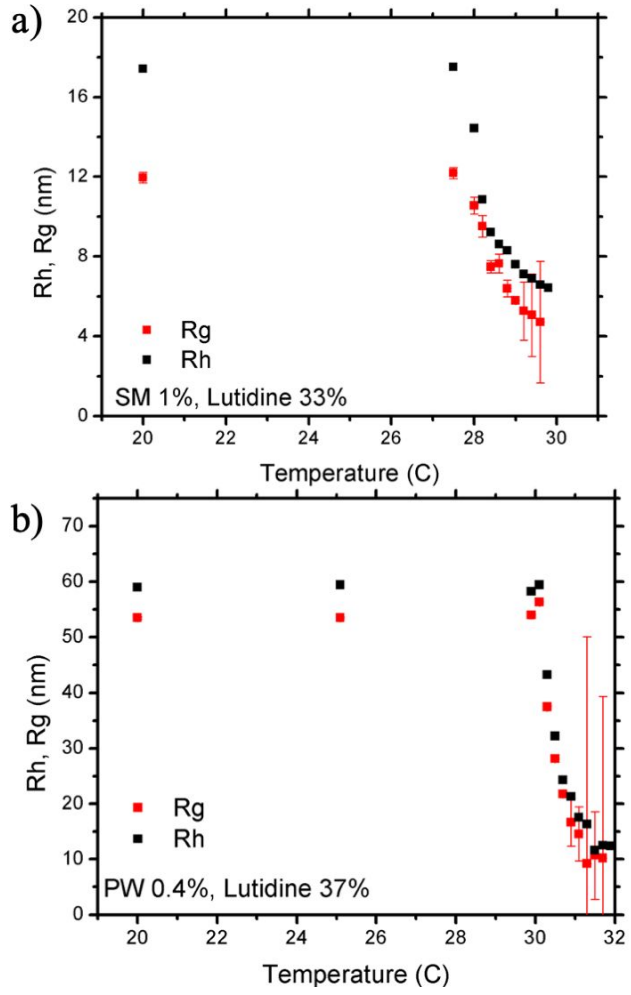

Figure 5. a) Radius of gyration, R_g, and hydrodynamic radius, Rh, determined through SANS and DLS, respectively, for P1 silica particles in solution after the purification. b) Radius of gyration, R_g, and hydrodynamic radius, Rh, determined by SANS and DLS, respectively, for P2 silica particles in solution after the purification. The error bars represent one standard deviation. In some cases the error bars are smaller than the symbol.

- USING LIGHT SCATTERING TO IDENTIFY T_a AND $\Delta T_p(w)$

To apply this purification method, we need to first identify w, $T_a(w)$, and $\Delta T_p(w)$. In this paper, we use the *in situ* SANS measurements to determine these parameters. However, SANS is only available at national facilities. We here show that static light scattering (SLS) can be used to determine these parameters. SLS only measures the scattering intensity from a sample. Our DLS can report the scattering intensity as a function of time and temperature. Therefore, it can be used as a fixed angle static light scattering instrument too.

Figure 6a) shows the SLS intensity as a function of the temperature for P1 samples. At the beginning, the intensity slowly increases due to the aggregation of silica particles. However, when reaching about 28.2 °C, the intensity starts decreasing. Comparing with our in-situ SANS experiment, this is the temperature point at which aggregated particles start precipitating out of solutions. The intensity reaches a minimum at about 30 °C. Again, comparing

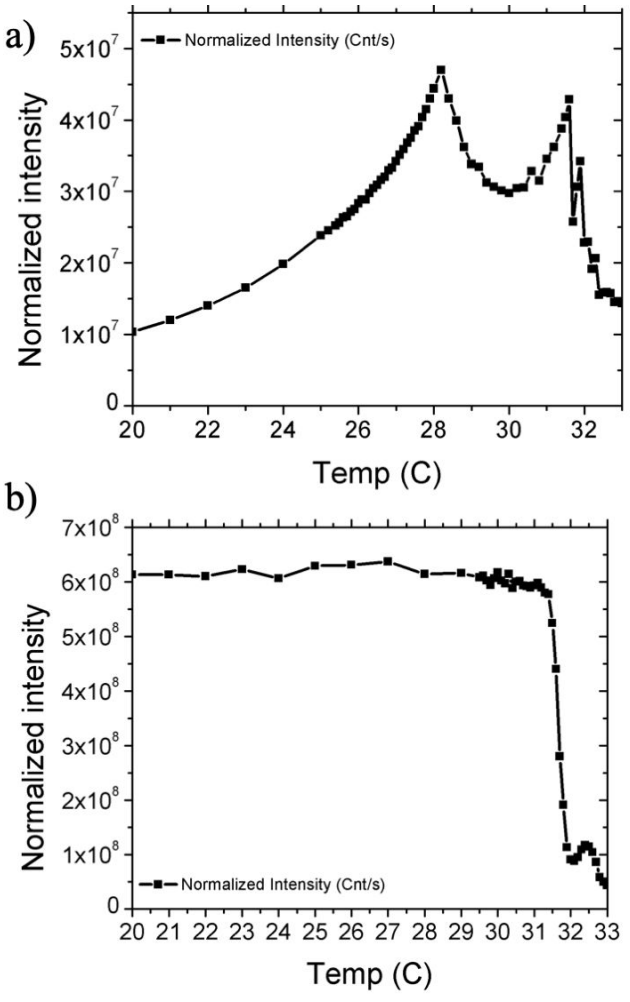

Figure 6. a) Normalized intensity for P1 silica particles at 1% volume fraction immersed in lutidine/water mixture at 33% mass fraction, as function of temperature. b) Normalized

intensity for P2 silica particles at 0.4% volume fraction immersed in lutidine/water mixture at 37% mass fraction, as function of temperature.

with Fig. 2a) from SANS measurements, this is the temperature at which most silica particles precipitate out of solutions. Therefore, we can assign this temperature to be $T_e(w)$. Hence, for this sample, T_a=28.2°C, $\Delta T_p(w)$=1.8 °C. The SLS intensity keeps increasing after reaching the minimum. This is due to the increased density fluctuation of the binary solvent when the temperature approaches the solvent spinodal line. (Note that the phase separation temperature of the bulk solvent is higher than T_e as shown schematically in Figure 1.) Thus, the second peak at slightly over 31 °C is related with the liquid-liquid phase separation of the binary solvent. Due to the use of D_2O in the solvent, the phase separation temperature of this solvent is lower than that of the binary solvent prepared using H_2O.

We also performed the SLS experiment for P2 samples. The SLS intensity does not change too much below 30.0 °C as shown in Fig. 6b). However, for temperatures larger than 30.0°C when particles start to aggregate, the normalized intensity starts to slightly fluctuate as the consequence of the aggregation process. In the temperature window from 31.5 °C to 32.0°C, the intensity abruptly falls down which is associated with the particle precipitation in the laser beam and is consistent with the change of the scatterings patterns in Fig. 3a), where in the same temperature range the scattering intensity changes significantly.

For both samples, P1 and P2, from Fig. 6 it is clear that the use of SLS can be a quick method to determine $T_a(w)$ and $\Delta T_p(w)$, which are critical parameters for this purification process. By investigating the $T_a(w)$ and $\Delta T_p(w)$ as a function of w, the optimum lutidine concentration for the purification method can be determined using the SLS. The use of SLS for this purpose offers a cost-effective method because light scattering instruments are available as a standard equipment in many laboratories compared with neutron scattering instruments that are only available at national facilities.

CONCLUSIONS

Employing SANS and DLS we demonstrated that a generic method of the particle size purification method is efficient to separate small particles from the bigger ones for silica particles with a large polydispersity. We demonstrate here that even when the CCF introduced attraction is short ranged compared with the particle diameter, the aggregation is still highly size sensitive. This result is very significant. Particles with a short-ranged attraction have been model systems to study a wide range of scientific problems. Size polydispersity are usually introduced in those studies to avoid the crystal formation. And also for many applications of colloidal systems, the size polydispersity is inevitable. Our results imply that the aggregation formation can be highly size sensitive for all these systems. In fact, combining the results from both small and large particle systems demonstrated here, this size sensitivity is true for both short-ranged and long-ranged attraction.

We also demonstrate that this purification method works equally well at higher particle concentrations that can greatly increase the purification efficiency. However, to have a wide temperature range for the purification process, i.e. to widen $\Delta T_p(w)$, the lutidine concentration of the binary solvent needs to be adjusted for different particle concentrations. In general, there is an optimum lutidine concentration to have the largest $\Delta T_p(w)$. In order to maintain the same $\Delta T_p(w)$ when increasing the particle concentration, the lutidine concentration in the binary solvent needs to be decreased as the particles studied here favor water in the binary solvent.

The key of this method is to choose the composition of the binary solvent, i.e., the lutidine concentration in this study, and the temperature control range. By sensitively controlling the temperature, we can, step by step, introduce the aggregation of larger particles through solvent mediated interaction to allow big particles precipitate when they form aggregates. By separating the precipitates, the particles left in the solutions have a better size monodispersity. This is a relatively cost effective method of the particle size purification. As the CCF is a generic solvent induced force for particles dispersed in a binary solvent, this method can be potentially extended to many kinds of particles and different types of binary solvents. Furthermore, we show that light scattering can serve as a useful tool to identify key parameters for this purification method. It would be interesting to further study the effect of the particle shape, such as rod and ellipsoid, and surface chemistry on the efficiency of this purification method. [24, 41] Since the critical temperature for different types of binary solvents can vary significantly, the temperature range of this purification method can thus be controlled and extended to different temperature regions by properly choosing a binary solvent.

AUTHOR INFORMATION

Corresponding Author

* E-mail: yunliu@udel.edu or yunliu@nist.gov

Author Contributions

The manuscript was written through contributions of all authors. / All authors have given approval to the final version of the manuscript. / ‡These authors contributed equally. (match statement to author names with a symbol)

Funding Sources

US National Science Foundation under Agreement No. DMR-1508249
Conacyt (Grant. No. 237425)

ACKNOWLEDGMENT

Access to NGB30mSANS was provided by the Center for High Resolution Neutron Scattering, a partnership between the National Institute of Standards and Technology and the National Science Foundation under Agreement No. DMR-1508249. Certain commercial equipment, instruments, or materials (or suppliers, or software, ...) are identified in this paper to foster understanding. Such identification does not imply recommendation or endorsement by the National

Institute of Standards and Technology, nor does it imply that the materials or equipment identified are necessarily the best available for the purpose. J.R. Villanueva-Valencia acknowledge to the National Council of Science and Technology (CONACYT) for the fellowship provided to develop this research. J.R. Villanueva-Valencia and R. Castañeda-Priego also acknowledge partial financial support from CONACYT (Grant. No. 237425)

REFERENCES

[1] C. M. Dobson, *Nature,* vol. 426, pp. 884-890, 2003.

[2] S. H. El-Gohary, M. K. Metwally, S. Eom, S. H. Jeon, K. M. Byun and T.-S. Kim, *Biomed. Eng. Lett.,* vol. 4, p. 250, 2014.

[3] Y. Pu, W. Wang, G. Tang, R. Alfano, M. Xu and J. A. Eastham, *J. Biomed. Opt.,* vol. 4, no. 8, p. 081419, 2012.

[4] T. Brown, P. D. Dalton and D. W. Hutmacher, *Prog. Polym. Sci,* vol. 56, pp. 116-166, 2016.

[5] S. L. Wingstrand, N. J. Alvarez, Q. Huang and O. Hassager, *Phys. Rev. Lett.,* vol. 115, p. 078302, 2015.

[6] N. Tasios, J. R. Edison, R. van Roij, R. Evans and M. Dijkstra, *J. Chem. Phys.,* vol. 145, p. 084902, 2016.

[7] N. Valadez-Perez, Y. Liu and R. Castañeda-Priego, *Phys. Rev. Lett.,* vol. 120, no. 24, p. 248004, 2018.

[8] Y. Liu and Y. Xi, *Curr. Opin. Colloid Interface Sci.,* vol. 39, pp. 123-136, 2019.

[9] P. D. Godfrin, I. E. Zarraga, J. Zarzar, L. Porcar, P. Falus, N. J. Wagner and Y. Liu, *J. Phys. Chem. B,* vol. 120, pp. 278-291, 2016.

[10] C. Likos, *Phys. Rep.,* vol. 348, p. 267, 2001.

[11] S. Oosawa and F. Asakura, *J. Chem. Phys.,* vol. 22, p. 1255, 1954.

[12] A. Vrij, *Pure Appl. Chem,* vol. 48, p. 471, 1976.

[13] D. Beysens and D. Esteve, *Phys. Rev. Lett.,* vol. 54, p. 2123, 1985.

[14] C. Hertlein, L. Helden, A. Gambassi, S. Dietrich and C. Bechinger, *Nature,* vol. 451, pp. 172-175, 2008.

[15] S. G. Stuij, M. Labbé-Laurent, T. E. Kodger, A. Maciolek and P. Schall, *Soft Matter,* vol. 13, p. 5233, 2017.

[16] N. Tasios and M. Dijkstra, *J. Chem Phys.,* vol. 146, p. 134903, 2017.

[17] P. Gallagher and J. Maher, *Phys. Rev. A,* vol. 46, p. 2012, 1992.

[18] F. Shlesener, A. Hanke and S. Dietrich, *J. Stat. Phys,* vol. 110, no. 3-6, 2003.

[19] A. Hanke, F. Schlesener, E. Eisenriegler and S. Dietrich, *Phys. Rev. Lett.,* vol. 81, no. 9, pp. 1885-1888, 1998.

[20] A. Maciolek and S. Dietrich, *Rev. Mod. Phys,* vol. 90, p. 045001, 2018.

[21] R. Okamoto and A. Onuki, *Phys. Rev. E: Stat., Nonlinear, Soft Matter Phys.,* vol. 88, p. 22309, 2013.

[22] T. W. Burkhardt and E. Eisenriegler, *Phys. Rev. Lett.,* vol. 74, pp. 3189-3192, 1995.

[23] C. Yu, J. Zhang and S. Granick, *Angew. Chem. Int. Ed. Engl.,* vol. 53, pp. 4364-4367, 2014.

[24] T. Nguyen, A. Newton, S. Veen, D. Kraft, P. Bolhuis and P. Shall, *Adv. Mater.,* vol. 29, p. 1700819, 2017.

[25] M. Fisher and P. de Gennes, *C. R. Acad. Sc. Paris,* vol. t. 287, pp. 207-209, 1978.

[26] D. Boon, J. Otwinowski, S. Sacann, H. Guo, G. Wegdam and S. P., *Phys. Rev. Lett.,* vol. 103, p. 156101, 2009.

[27] P. J. Upton, J. Indekeu and J. Yeomans, *Phys. Rev. B,* vol. 40, pp. 666-679, 1989.

[28] M. Dang, A. Verde, V. Nguyen, P. Bolhuis and P. Shall, *J. Chem. Phys.,* vol. 139, p. 094903, 2013.

[29] H. Guo, G. Stan and Y. Liu, *Soft Matter,* vol. 14, pp. 1311-1318, 2018.

[30] T. Mohry, S. Kondrat, A. Maciolek and S. Dietrich, *Soft Matter,* vol. 10, pp. 5510-5522, 2014.

[31] C. E. Bertrand, P. D. Godfrin and Y. Liu, *J. Chem. Phys.,* vol. 143, p. 084704, 2015.

[32] Z. Wang, H. Guo, Y. Liu and X. Wang, *J. Chem. Phys.,* vol. 149, p. 084905, 2018.

[33] M. Kotlarchyk, R. Stephens and J. Huang, *J. Phys. Chem.,* vol. 92, pp. 1533-1538, 1988.

[34] P. Gallagher, L. Kurnaz and J. Maher, *Phys Rev. A,* vol. 46, p. 7750, 1992.

[35] H. Grüll and D. Woermann, *Ber. Bunsenges Phys. Chem.,* vol. 101, p. 814, 1997.

[36] B. Rathke, H. Grüll and D. Woermann, *J. Colloid Interface Sci.,* vol. 192, p. 334, 1997.

[37] M. Fukoto, Y. Yano and P. Pershan, *Phys. Rev. Lett.,* vol. 94, p. 135702, 2005.

[38] S. Rafaï, D. Bonn and J. Meunier, *Physica A,* vol. 386, p. 31, 2007.

[39] P. Godfrin, N. Valadez-Perez, R. Castañeda-Priego, N. Wagner and Y. Liu, *Soft matter,* vol. 10, no. 28, pp. 5061-5071, 2014.

[40] N. Valadez-Perez, A. Benavides, E. Schöll-Paschinger and R. Castañeda-Priego, *J. Chem. Phys.,* vol. 137, no. 8, p. 084905, 2012.

[41] M. Labbé-Laurent, A. D. Law and S. Dietrich, *J. Chem. Phys.* , vol. 147, p. 104701, 2017.